AIMS Materials Science, 3(2): 620-633.
DOI: 10.3934/matersci.2016.2.620
Received: 14 April 2016
Accepted: 23 May 2016
Published: 25 May 2016

http://www.aimspress.com/journal/Materials

Research article

Assessment of extrusion-sonication process on flame retardant polypropylene by rheological characterization

Guadalupe Sanchez-Olivares [1,*], Fausto Calderas [1], Antonio Sanchez-Solis [2], Luis Medina-Torres [3], Leonardo R. Moreno [2], and Octavio Manero [2]

[1] CIATEC, A.C., Omega 201, León, Gto. 37545, Mexico
[2] Instituto de Investigaciones en Materiales, Universidad Nacional Autónoma de México, Avenida Universidad 3000, Mexico city 04510, Mexico
[3] Facultad de Química, Universidad Nacional Autónoma de México, Avenida Universidad 3000, Mexico city 04510, Mexico

* **Correspondence:** E-mail: gsanchez@ciatec.mx; Tel: 52-4777100011.

Abstract: In this work, the rheological behavior of flame retardant polypropylene composites produced by two methods: 1) twin-screw extrusion and 2) ultrasound application combined with a static mixer die single-screw extrusion is analyzed in detail; results are related to the morphology of the composites. The flame retardant polymer composites are composed of a polypropylene matrix, an intumescent flame retardant system and functionalized clay. Scanning electron microscopy revealed that the combination of the static mixer die and on-line sonication reduced particle size and improved the dispersion and distribution of the intumescent additives in the polypropylene matrix at the micrometric level. From linear viscoelastic properties, the Han, Cole-Cole and van Gurp-Palmen diagrams characterized the improved particle dispersion of the flame retardant additives. Two well-defined rheological behaviors were observed in these diagrams. These behaviors are independent on clay presence and concentration. In fact, the ultrasound device generates a 3D highly interconnected structure similar to a co-continuous pattern observed in polymer blends as evidenced by rheological measurements. This improvement in the dispersion and distribution of the additives is attributed to the combined effect of the static mixer die and on-line sonication that allowed reducing the additive content while achieving the optimum classification UL94-V0.

Keywords: rheological properties; extrusion-sonication; ultrasound; flame retardant; composites

1. Introduction

According to the usual method to produce flame retardant polymer materials, large additive concentrations are normally employed to obtain the desired properties; for example V0 according to UL-94 classification. However, increasing additive concentration in a polymer matrix is accompanied with processing problems and poor mechanical properties of the materials caused by low degree of dispersion and agglomeration of the additives, usually. Specific novel solutions, such as the production of nanocomposite materials under ultrasonic vibrations, are currently studied in polymer melt extrusion to improve distribution and dispersion of the particles in the polymer matrix [1–4].

The degree of the dispersion and distribution of the flame retardant additives has a large impact on the rheological, mechanical and flame retardant properties of the polymer matrix [5,6]. In polymer processing, rheological properties are quite important for the characterization of the polymer structure; for example, the Cole-Cole (η'' versus η'), Han (G' versus G'') and van Gurp-Palmen (delta versus |G*|) diagrams have been widely used to analyze rheological data. Chen et al. [7] constructed the Cole-Cole diagram to infer the effect of ultrasonic vibrations on the HDPE-PS blend, and they found that the zero-shear viscosity (η_0) diminished after sonication during melt extrusion. Changes in the molecular structure, including degradation of the HDPE-PS blend upon ultrasound application were revealed by molecular weight measurements. Using the Han diagram, Kim et al. [8] determined a long-chain branched structure in the polypropylene matrix caused by high-intensity ultrasound waves. An enhanced elasticity associated to the presence of a G' frequency-independent plateau (G' > G'') was related to an inter-connected physical structure. With regard to polymer nanocomposites, the Han diagram has been used to determine nanoparticle-polymer matrix interactions. For example, Lai et al. [9] studied the effect of modified silica in a polyethylene matrix and they found that the materials with high concentrations of non-treated silica (>5 phr) deviate from the reference with low silica contents, indicating low compatibility or agglomerate formation. The rheological data of the materials produced with modified silica enabled the construction of master curves over the whole range of concentration, in fact revealing improved compatibility.

In this work, the morphological, flame retardant and rheological properties of polypropylene based composites are reported. Intumescent flame retardant additives were incorporated in the produced materials using two different extrusion processes, twin screw (a traditional process) and single screw applying ultrasonic vibrations on a specific static mixer die. This static mixer die has a unique design to promote extensional flow by including compression-decompression zones that also produce intensive mixing; the details of equipment, processing condition and procedures have been reported in a previous work [5], where the morphology, thermal stability, flame retardant and mechanical properties were studied in detail. The main objective of this work is the assessment of the particle dispersion and composite microstructure using the extrusion-sonication on-line process through the resulting rheological and morphological properties of the materials.

2. Materials and Method

2.1. Materials

The following components were used to obtain the materials: medium-impact polypropylene copolymer (PP) from Indelpro (Mexico) with 4.0 g/10 min according to ASTM D1238 melt flow

index; sodium bentonite clay, from Clariant (former Süd-Chemie) with 55 meq/100g ion interchange capacity; L-lysine mono-chlorohydrated aminoacid and maleic anhydride. The intumescent flame retardant system is composed of pentaerythritol with a purity of 94–95%; melamine with a purity of 99.8% and ammonium polyphosphate from Clariant (trade name Exolit APP 422) with phosphorous content of 31–32 wt.% and molecular weight n > 1000 where n = number of phosphate units $(NH_4PO_3)n$. The average particle sizes of the intumescent additives according to suppliers are: ammonium polyphosphate: $D_{50} < 15$ microns and melamine and prentaerythritol: $D_{50} < 40$ microns.

2.2. Equipment

The materials were obtained by two methods: traditional extrusion using a twin screw counter-rotating Leistritz Micro 27 extruder with diameter of 27 mm and L/D of 32 and extrusion with on-line sonication using a single screw extruder with diameter of 25.4 mm and L/D of 24 coupled to a static mixer die; this extrusion process (single screw) was assisted by a set of 6 piezoelectric elements to generate ultrasonic vibrations with a frequency of 40 kHz, 100 V amplitude and 300 W power applied in the region were extensional flow is produced (patent under revision). The injection molding process was carried out in a Demag Ergotech 50–200 injection molding machine.

2.3. Synthesis

Bentonite clay was functionalized through cation-ion interchange reactions using L-lysine aminoacid as intercalant agent [10,11,12]. Polypropylene grafted with maleic anhydride via reactive extrusion was used to improve matrix-clay compatibility, according to the process of Shi et al. [13]. Grafted polypropylene/functionalized-clay proportion was kept at 2:1 ratio.

2.4. Extrusion process

Table 1 shows the overall data of the materials produced, including the extrusion conditions, intumescent flame retardant additives and functionalized clay content. The additives that form the intumescent system (pentaerythritol, melamine and ammonium polyphosphate) were added maintaining the same constant mass ratio, 1:1:1; for example, 30 phr of intumescent flame retardant is composed by 10 phr of pentaerythritol, 10 phr melamine and 10 phr of ammonium polyphosphate. For the case of 21 phr of intumescent flame retardant, each additive content is 7 phr. Samples are identified according to the following codes: in the sample identification code IFR 21-CLAY 3/Sonicated, IFR means Intumescent Flame Retardant, 21 means 21 phr (parts per hundred of resin) of intumescent additives, CLAY 3 means functionalized clay concentration (3 phr) and Sonicated stands for the single screw-sonicated extrusion process (sonicated materials). Rotational speed for non-sonicated materials, in a twin-screw extruder, was 200 rpm. For sonicated materials, the single-screw extruder rotational speed was 30 rpm. Ultrasonic vibrations (on-line sonication) were applied with a frequency of 40 kHz, 100 V amplitude and 300 W power. These processing parameters were determined previously [14]. The sonication applied to molten polymers has an important effect when the polymer is near or in contact with the emission source, producing cavitation, “jet” flows, molecular chains scission, disentanglement, and so on. In the system employed in this work, the static mixer die coupled to the single screw extruder has compression-decompression zones,

promoting extensional flows, where molten polymer goes through a very narrow aperture (0.6 mm); at this point, ultrasound-waves produced by the ultrasound transducers are applied to the polymer. These process conditions produce a substantial effect on the flow properties of the composite [15,16].

Table 1. Materials description.

Sample identification	Conditions process	Intumescent flame retardant content [phr]	Modified clay content [phr]
IFR 30	Non-sonicated	30	0
IFR 21	Non-sonicated	21	0
IFR 21-CLAY 1	Non-sonicated	21	1
IFR 21-CLAY 3	Non-sonicated	21	3
IFR 30/Sonicated	Sonicated	30	0
IFR 21/Sonicated	Sonicated	21	0
IFR 21-CLAY 1/Sonicated	Sonicated	21	1
IFR 21-CLAY 3/Sonicated	Sonicated	21	3

2.5. Characterization

Rheological tests were performed in a stress-controlled TA-G2 rheometer using the parallel plates fixture with 25 mm diameter and a heating chamber (TA-Extended Temperature System). All rheological tests were carried out at 215 °C in the linear viscoelastic regime. Micrographs were taken in a field-emission scanning electron microscope (SEM) Jeol JSM-7600F. Flame retardant properties in vertical position UL94-V were evaluated according to ASTM D3801 (IEC 707-9 and ISO 1210).

3. Results and Discussion

3.1. Morphology

In Figure 1, the scanning electron microscopy micrographs of fractured surfaces for IFR 30 and IFR 21-CLAY 1 non-sonicated materials are shown. These materials contain 30 phr of intumescent flame retardant system (Figure 1-A) and 1 phr functionalized clay with 21 phr of intumescent flame retardant system (Figure 1-C) respectively. In these non-sonicated materials large particle agglomerates (around 30 microns size) are observed. The morphology of these compounds obtained by the traditional extrusion process (twin screw) shows the difficulty to distribute and disperse large contents of intumescent flame retardant additives into the polymer matrix. On the other hand, in Figure 1 B and D, the morphology of the sonicated materials is shown (IFR 30 and IFR 21-CLAY 1 respectively). Here, much better dispersion and distribution of the particles are observed with particle sizes around one micron. Thus these micrographs of fractured surfaces clearly show the effect of the on-line sonication on the morphology of the samples rendering an improved dispersion and

distribution of the flame retardant additive particles in the polymer matrix. Functionalized clay particles are not observed or distinguishable in the SEM micrographs; probably by their low content (1 phr) or they could possibly be well dispersed at nanometric level and hence outside of the resolution of the SEM.

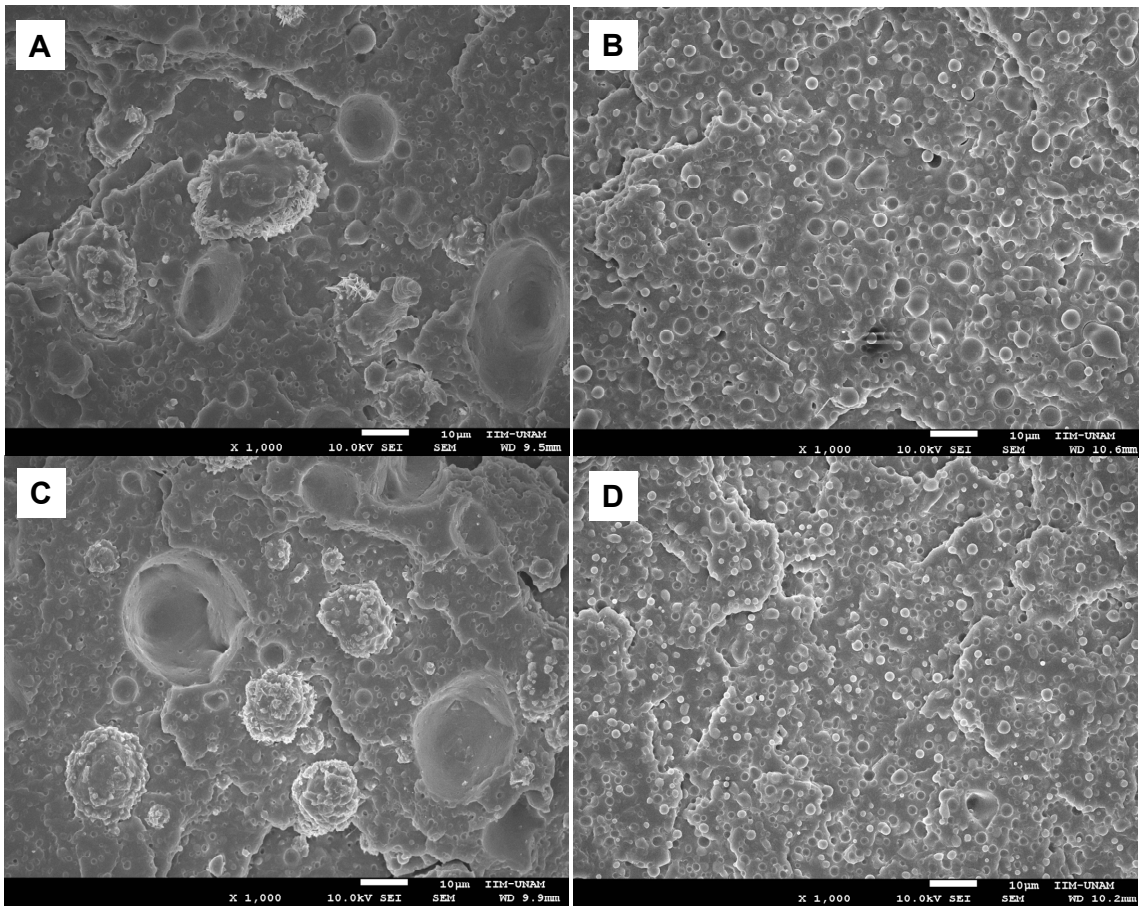

Figure 1. Scanning electron microscopy micrographs of fractures surfaces: A**)** IFR 30, B) IFR 30/Sonicated, C) IFR 21-CLAY 1 and D**)** IFR 21-CLAY 1/Sonicated.

3.2. Flame retardant properties

The procedure to test the flame retardant properties was carried out according to the vertical position UL94 classification. Results (Table 2) show the effectiveness of the intumescent flame retardant system when a concentration of 30 phr is used. The non-sonicated and sonicated materials obtained at this particular concentration (IFR 30/Sonicated and IFR 30) render an optimum V0 classification. These results are not surprising considering that at high concentrations the intumescent flame retardant system is very effective [17]. However, when the concentration is reduced to 21 phr, no flame retardant classification is obtained for the different materials prepared with exception of the compound IFR 21-CLAY 1/Sonicated, which rates V0 classification. This particular result is attributed to the distribution and dispersion action of the combined on-line sonication and static mixer die process upon a material that contains 1 phr of functionalized clay. When clay particles are properly dispersed and distributed (usually at nanometric level) they form a barrier-layer on the

surface of the material under combustion which isolates the material reducing the heat and mass transfer, in fact decreasing the flammability of the material [18]. However, in some systems, when clay particles are not well dispersed and/or exfoliated (larger clay contents are more difficult to disperse and/or exfoliate) a negative effect in the heat release rate is observed [19]. This is indeed the case for the 3phr clay sonicated material (IFR 21-CLAY 3/Sonicated) where no UL94-V0 rating was achieved.

Table 2. UL94 classification of the evaluated materials.

Sample identification	UL94 Clasification
PP	HB
IFR 30	V0
IFR 21	HB
IFR 21-CLAY 1	HB
IFR 21-CLAY 3	HB
IFR 30/Sonicated	V0
IFR 21/Sonicated	HB
IFR 21-CLAY 1/Sonicated	V0
IFR 21-CLAY 3/Sonicated	HB

3.3. Rheological properties

In Figure 2, the complex viscosity is plotted versus angular frequency. The sonicated materials (processed with single screw extrusion and the static mixer die) have larger viscosity values than the non-sonicated ones (processed with twin screw extrusion). This behavior reveals that degradation due to ultrasound vibrations at these processing conditions is not substantial. At low frequency (lower than 1.0 rad/s) a Newtonian region is apparent, while for high frequency (larger than 10 rad/s) the viscosity diminishes substantially. It is interesting that, the sample with 30 phr (IFR 30) shows the lowest viscosity of all samples which may be caused by polymer degradation due to the combination of high load of intumescent system (high shear stresses imposed on the compound leading to chain scissions) and lower dispersion as compared to the sonicated systems; this is indeed a problem with fire retardant polymer systems in which highly loaded compounds have good fire retardant properties but poor mechanical properties due to degradation effects [20]. Another interesting effect observed in the non-sonicated materials is the reduction in viscosity with the clay content, i.e., IFR 21-CLAY 1 material having higher viscosity than FR 21-CLAY 3. This effect has also been previously reported and may be attributed to clay particles having a lubricant effect when they are in a certain concentration absorbing enough high molecular weight polymer chains on the surface to cause a decrease in viscosity [21].

For the case of the sonicated materials, on-line sonication induces less pronounced shear thinning in the complex viscosity, revealing a more structured system which strongly depends on the effect of ultrasound rather than the composition of the materials. The increase in zero shear viscosity according to the Cox-Merz rule (not shown here) would indicate larger numbers of particle matrix interactions which would result from a more finely dispersed system as micrographs have shown. In the case of polymer nanocomposites, some authors have attributed the increase in the complex viscosity to a better dispersion and distribution of the nanoparticles in the polymer matrix, due to enhanced polymer–nanoparticle interactions [22]. In this case, it is likely that a smaller particle size or larger surface area of the particles together with better dispersion and distribution due to on-line sonication induces an increase in the viscosity. An increase in the shear-thinning behavior under simple shear has been observed in nanocomposites with the nanoparticles having a large aspect ratio and thus being more easily shear-oriented [23].

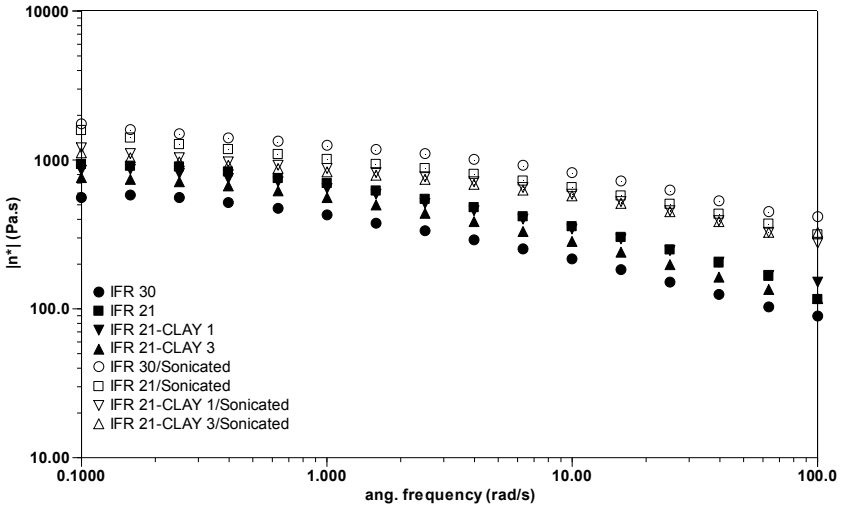

Figure 2. Complex viscosity versus frequency of non-sonicated materials (filled symbols) and sonicated ones (open symbols).

In Figure 3a, the storage modulus as a function of frequency is plotted for all materials. At high frequencies, all the sonicated materials show a larger storage modulus evidencing a more elastic structure produced by on-line sonication which is attributed to an increase in the entanglement density, due to the degree of dispersion of the particles (intumescent flame retardant system) in the polymer matrix [4,22]. For the sonicated materials, the storage modulus shows a slope lower than the limiting value of 2 in the terminal region, in fact revealing enhanced polymer-particle interactions ascribed to a tendency to, but not definitive, solid-like behavior as frequency diminishes. To further show this effect, Figure 3b shows a comparison between a sonicated material (IFR 21-CLAY 1/Sonicated) and a non-sonicated one (IFR 21-CLAY 1) with the same additive contents. Although there is no well-defined solid like region for the sonicated material, there is an obvious change of slope in the terminal region for all sonicated samples. For intumescent systems having particles with low aspect ratios, the interactions are increased but at a lower level as compared to highly filled exfoliated nanocomposites [23].

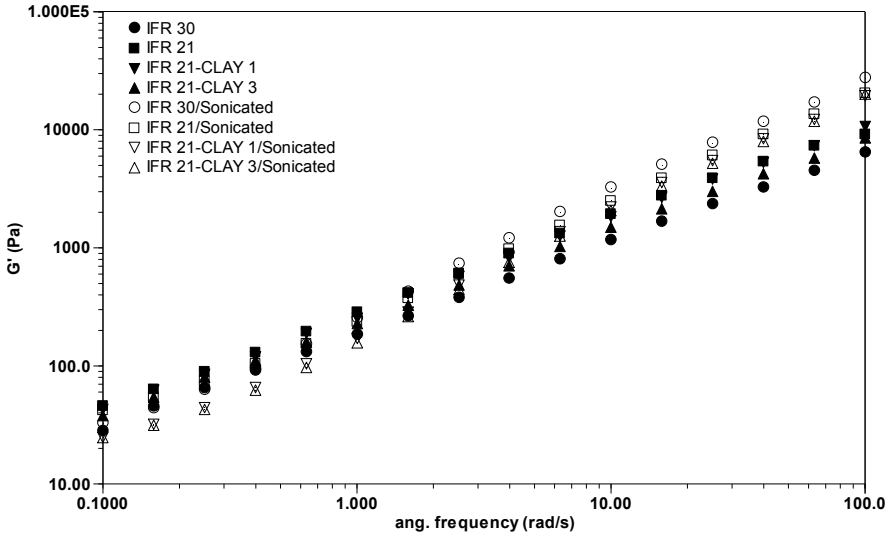

Figure 3a. Storage modulus as a function of the frequency of non-sonicated materials (filled symbols) and sonicated ones (open symbols).

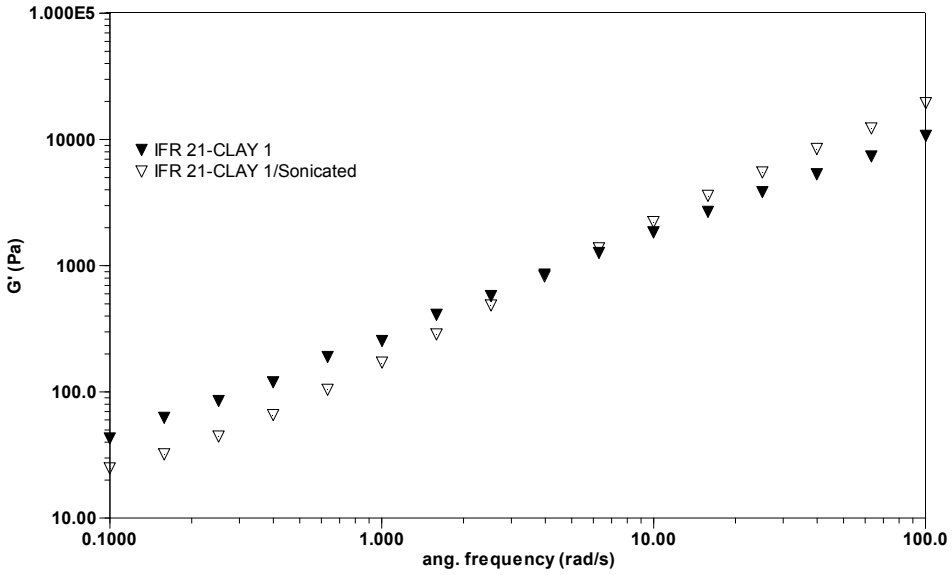

Figure 3b. Storage modulus as a function of the frequency of the IFR 21-CLAY 1 and IFR 21-CLAY 1/Sonicated materials.

In Figure 4a, the Han Diagram (G' vs G'') was prepared from linear viscoelastic data; surprisingly, two well defined master curves are observed, one for sonicated materials and one for non-sonicated ones, indicating the effect of the ultrasound on the materials. It has been reported that an increase in the slope of the G' vs G'' curve in the low frequency range indicates that the dispersed phase particle size decreases and the particle size distribution narrows [7,24]. In Figure 4a, both sets of curves show slopes that reduce with the lowering of frequency. This effect has been reported as evidence of strong elastic behavior [9] and in this case it would indicate particle-matrix interactions. The latter is reinforced by results shown in Figure 4b, where the slopes at low frequencies of the curves in Figure 4a are observed to be essentially linear and their numerical slope values are shown

in Table 3. A larger slope indicates that the particle size is reduced and particle size distribution narrows in polymer blends [7]. A slope with value closer to unity has been reported to be associated to improved interfacial interactions in polymer rubber blends [25]. In this work, the fact that the IFR 30/Sonicated curve is not only the curve with the largest slope but also the closest to a unit value suggests it to be the most homogeneous system. This result confirms that on-line sonication induces homogeneity (dispersion and distribution) of the particles (clay and intumescent system particles) as confirmed by the increasing slope from the lowest value observed in the non-sonicated materials. In addition, it has been reported that the slope of the Han curves approaches to 2 in the isotropic region of polymer liquid crystals and the slope deviates to lower values in the nematic region [26], in fact confirming that increasing slopes are related to a more homogeneous (and disordered) system.

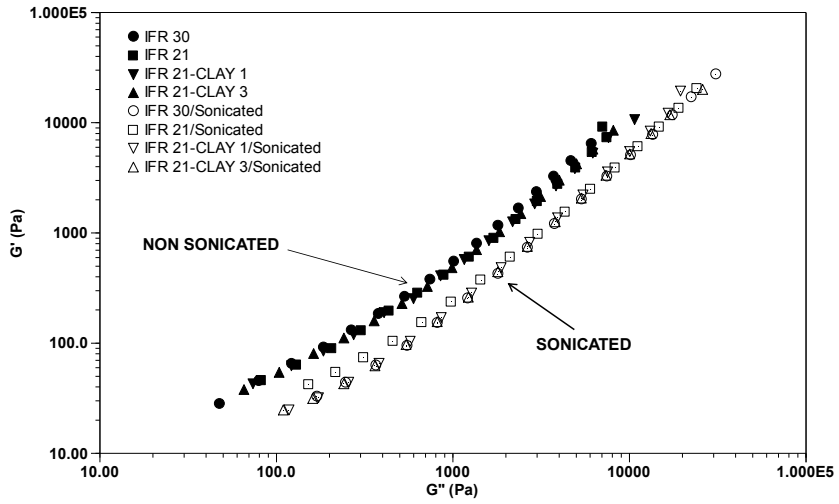

Figure 4a. Han diagram of non-sonicated materials (filled symbols) and sonicated ones (open symbols).

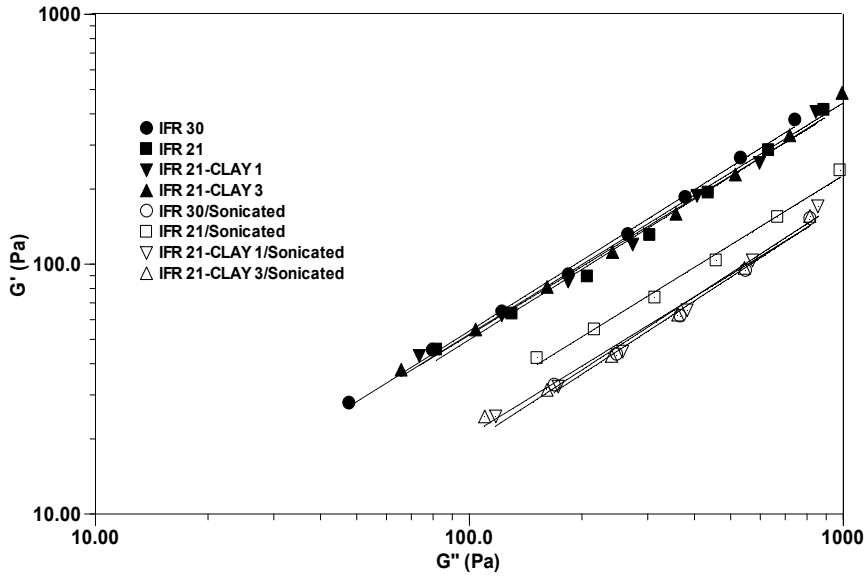

Figure 4b. Slopes in the low frequency region of the Han diagram (see Figure4a). The corresponding numerical values are shown in Table 3.

Table 3. Values of the slope in the low frequency region of the Han diagram.

Sample identification	Numerical slope values
IFR 30	0.940
IFR 21	0.935
IFR 21-CLAY 1	0.912
IFR 21-CLAY 3	0.926
IFR 30/Sonicated	0.977
IFR 21/Sonicated	0.925
IFR 21-CLAY 1/Sonicated	0.973
IFR 21-CLAY 3/Sonicated	0.920

Figure 5 shows the Cole-Cole diagram (η'' vs η') for the non-sonicated materials and Figure 6 discloses data for the sonicated ones. The non-sonicated materials tend to deviate from a semicircular shape indicating poor compatibility due to strong particle-particle interactions [27,28,29]. Although the sonicated materials do not show a smooth semicircular and well-defined shape in the Cole-Cole graph, the concavity presented in the curves is considered here as a sign of increased homogeneity. In Figure 6, the maximum of the curve represents a dominant relaxation process usually observed in homogeneous systems, where a well-defined semicircular shape is associated with a single relaxation mode. The tendency to the semicircular shape of the curves for the sonicated materials is associated with the smaller particle size and enhanced particle dispersion observed in the sonicated materials morphology.

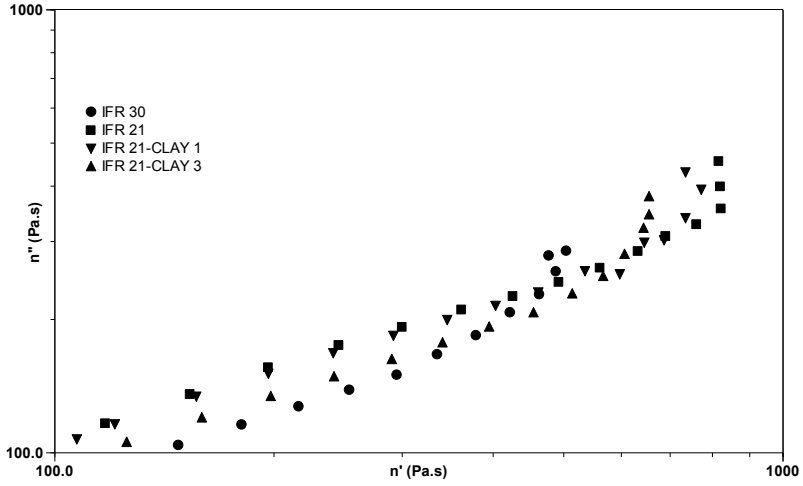

Figure 5. Cole-Cole diagram of non-sonicated materials.

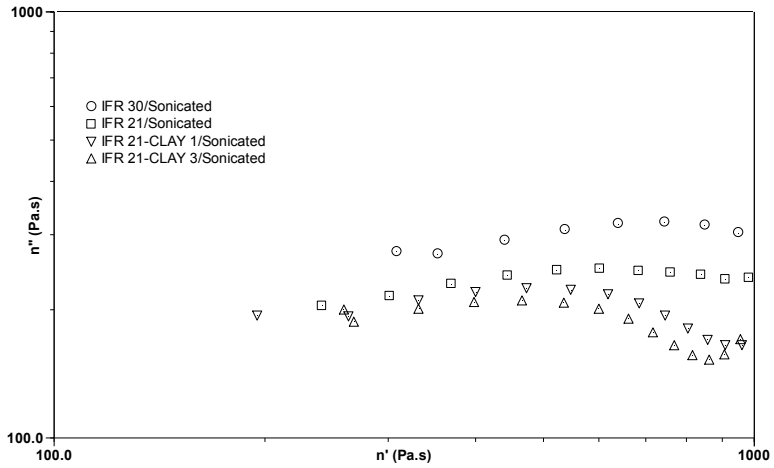

Figure 6. Cole-Cole diagram of sonicated materials.

Figure 7 shows the van Gurp-Palmen (vGP) diagram (delta versus |G*|) for the different materials studied in this work, where two master curves are clearly defined; sonicated and non-sonicated materials. Two structures are formed, as observed in the analysis of the Cole-Cole diagrams; the sonicated materials show enhanced polymer matrix-particle interactions (clay and intumescent flame retardant particles) due to the reduced particle size and improved dispersion and distribution of the particles. In contrast, in the non-sonicated materials, the structure is dominated by particle-particle interaction with larger particle size and poor distribution. As previously reported by Li et al. [30], when the structure of the blend is co-continuous, the vGP diagram shows a curve with a maximum and diminishes with decreasing values of the modulus |G*|, which is the case illustrated here for both unsonicated and sonicated materials. Li et al., also reported that when the structure is co-continuous, the Cole-Cole diagram shows a semicircular shape followed by a tail at high frequencies which correspond to the relaxation of the network formed by interpenetrating phases, which is observed in our results only for the sonicated samples (see Figure 6). This network is associated with a higher degree of interconnectivity between the phases [30].

Since the results highly resemble those of a co-continuous phase system, then a particular network structure is thought to be formed in the sonicated materials. This structure is generated by the size reduction of the particles and improved dispersion which increases drastically the free particle surface area and generates higher interconnectivity. The features observed for a droplet structure reported elsewhere [30,31], correspond to two semicircles in the Cole-Cole diagram (two characteristic relaxation mechanisms) and a plateau in the vGP diagram at low |G*| values. None of these features are observed in our results. Since the on-line sonication does not modify the interfacial tension between the phases, but only the distribution and particle size of the dispersed phase, the network behaves as that of a co-continuous polymer blend structure with a high degree of interconnectivity [31].

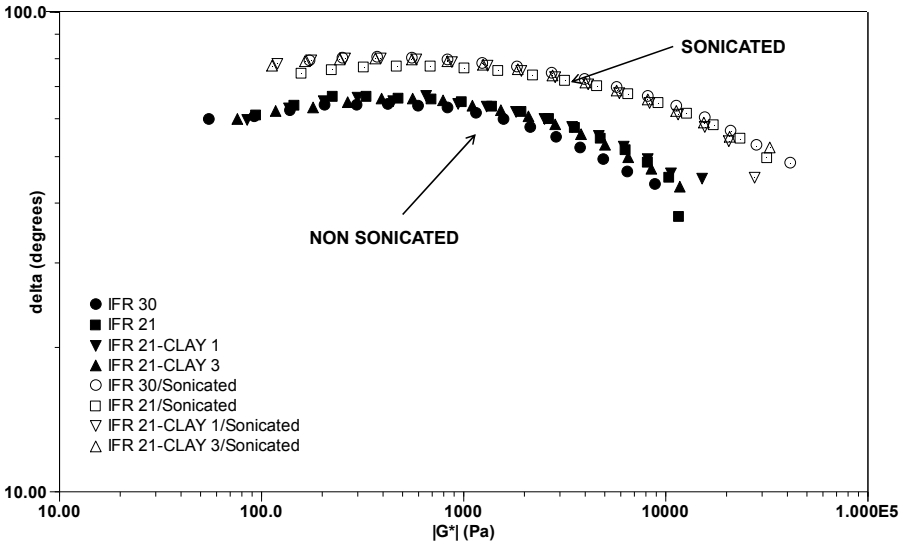

Figure 7. Van Gurp-Palmen diagram for non-sonicated materials (filled symbols) and for sonicated ones (open symbols).

4. Conclusion

In this study, the effect of on-line extrusion-sonication, using a static-mixing die, on the rheology of flame retardant compounds was analyzed in detail. From linear viscoelastic data the Han, Cole-Cole and van Gurp-Palmen diagrams indicated the improved dispersion of the sonicated materials as well as the particle size reduction of the intumescent system observed by SEM micrographs. Several interesting features were observed: the Han diagram revealed better particle dispersion brought about by a smaller particle size when sonication is applied; from the analysis of the slopes along the low-frequency region of this plot, a trend to a homogeneous material is observed as a result of improved dispersion of the intumescent additives. The Cole-Cole diagram also indicated improved particle dispersion, and from the van Gurp-Palmen diagram, a co-continuous interconnected structure similar to those observed in polymer blends is obtained using the on-line sonication process. Satisfactory flame retardant materials were obtained with 30 phr intumescent flame retardant additives content in both processes (materials with 30 phr obtained V0 classification). This is an expected result since high concentrations of intumescent system are commonly used to obtain good flame retardant properties. However, the effect of the single screw extrusion process with the static mixer die-sonication renders an improved level of dispersion and distribution of particles at the micrometric level, so that a reduction in the additive content from 30 to 21 phr with 1 phr clay, with the consequence of less processing problems at the compounding stage.

Acknowledgments

We thank the financial support from the GTO-2011-C04-167285, PAPIIT-UNAM and CONACYT 235880 projects. F.C. gratefully acknowledges financial fellowship support (Postdoctoral Grant CONACYT 235880 project). Also, we acknowledge the technical support of Dr. Omar N. Peralta (For the SEM analysis).

Conflict of Interest

The authors declare no conflicts of interest regarding this paper.

References

1. Horrocks AR, Kandola B, Milnes GJ, et al. (2012) The potential for ultrasound to improve nanoparticle dispersion and increase flame resistance in fibre-forming polymers. *Polym Degrad Stab* 97: 2511–2523.
2. Peng B, Wu H, Bao W, et al. (2011) Effects of ultrasound on the morphology and properties of propylene-based plastomer-nanosilica composites. *Polym J* 43: 91–96.
3. Li J, Zhao L, Guo SJ (2007) Ultrasound assisted development of structure and properties of polyamide 6/montmorillonite Nanocomposites. *J Macromol Sci B* 46: 423–439.
4. Zhong J, Isayev AI (2015) Properties of Polyetherimide/Graphite Composites Prepared Using Ultrasonic Twin-Screw Extrusion. *J Appl Polym Sci* 132.
5. Sanchez-Olivares G, Sanchez-Solis A, Calderas F, et al. (2013) Extrusion with ultrasound applied on intumescent flame-retardant polypropylene. *Polym Eng Sci* 53: 2018–2026.
6. Sanchez-Olivares G, Sanchez-Solis A, Calderas F, et al. (2013) Flame retardant high density polyethylene optimized by on-line ultrasound extrusion. *Polym Degrad Stab* 98: 2153–2160.
7. Chen G, Guo S, Li Y (2004) Dynamical rheological properties of high-density polyethylene/polystyrene blends extruded in the presence of ultrasonic oscillations. *J Appl Polym Sci* 92: 3153–3158.
8. Kim KY, Nam GJ, Lee SM, et al. (2006) Rheological properties of polypropylene modified by high-intensity ultrasonic sonic waves. *J Appl Polym Sci* 99: 2132–2137.
9. Lai SM, Huang CY, Li SC, et al. (2011) Preparation and properties of melt-mixed metallocene polyethylene/silica nanocomposites. *Polym Eng Sci* 51: 434–444.
10. Parbhakar A, Cuadros J M, Sephton A, et al. (2007) Adsorption of L-lysine on montmorillonite. *Colloid Surface A* 307: 142–149.
11. Cuadros J, Aldega L, Vetterlein J, et al. (2009) Reactions of lysine with montmorillonite at 80 ºC: implications for optical activity, H + transfer and lysine-montmorillonite binding. *J Colloid Interf Sci* 333: 78–84.
12. Kitadai N, Yokoyama T, Nakashima S (2009) In situ ATR-IR investigation of L-lysine adsorption on motmotillonite. *J Colloid Interf Sci* 338: 395–401.
13. Shi D, Yang J, Yao Z, et al (2001) Functionalization of isotactic polypropylene with maleic anhydride by reactive extrusion: mechanism of melt grafting. *Polym* 42: 5549–5557.
14. Ibarra-Macias DA (2013) Estudio de materiales compuestos de poli(tereftalato de etileno) y polipropileno asistidos por ultrasonido. M. Sc. Thesis, Universidad Nacional Autónoma de México. Available from: http://www.dgbiblio.unam.mx/index.php/catalogos.
15. Li J, Guo S, Li X (2005) Degradation kinetics of polystyrene and EPDM melts under ultrasonic irradiation. *Polym Degrad Stabil* 89: 6–14.
16. Li Y, Li J, Guo S, et al. (2005) Mechanochemical degradation kinetics of high-density polyethylene melt and its mechanics in the presence of ultrasonic irradiation. *Ultrason Sonochem* 12: 183–189.

17. Bourbigot S, Le Bras M, Duquesne S, et al. (2004) Recent advances for intumescent polymers. *Macromol Mater Eng* 289: 499–511.
18. Gilman JW, Jackson CL, Morgan AB, et al. (2000) Flammability Properties of Polymer-Layered-Silicate Nanocomposites. *Chem Mater* 12: 1866–1873.
19. Sanchez-Olivares G, Sanchez-Solis A, Camino G, et al. (2008) Study on the combustion behavior of high impact polystyrene nanocomposites produced by different extrusion processes. *Express Polym Lett* 2: 569–578.
20. Kiliaris P, Papaspyrides CD (2010) Polymer/layered silicate (clay) nanocomposites: An overview of flame retardancy. *Prog Polym Sci* 35: 902–958.
21. Calderas F, Sanchez-Solis A, Maciel A, et al. (2009) The transient flow of the PET-PEN-Montmorillonite clay nanocomposite. *Macromol Sympo* 283: 354–360.
22. Isayev AI, Kumar R, Lewis TM (2009) Ultrasound assisted twin screw extrusion of polymer-nanocomposites containing carbon nanotubes. *Polymer* 50: 250–260.
23. Li Q, Zeng Q, Huang Y, et al. (2013) Dispersion and rheology of polypropylene/organoclay nanocomposites: effect of cation exchange capacity and number of alkyl tails. *J Mater Sci* 48: 948–959.
24. Chen G, Guo S, Li H (2002) Ultrasonic improvement of the compatibility and rheological behvaior of high-density polyethylene/polystyrene blends. *J Appl Polym Sci* 86: 23–32.
25. Bagheri H, Jahani Y, Haghighi MN, et al. (2011) Dynamic shear rheological behavior of PP/EPR in-reactor alloys synthetized by Multi-stage Sequential Polymerization Process. *J Appl Polym Sci* 120: 3635–3641.
26. Kim SS, Han CD (1993) Effect of molecular weight on the rheological behavior of thermotropic liquid-crystalline polymer. *Macromolecules* 26: 6633–6642.
27. Kwak H, Rana D, Choe SJ (2000) Melt rheology of binary blends of metallocene polyethylene with conventional polyolefins. *J Ind Eng Chem* 6: 107–114.
28. Ahmed J, Varshney SK, Auras RJ (2010) Rheological and thermal properties of polylactide /silicate nanocomposites films. *J Food Sci* 75: 17–24.
29. Luan L, Wu W, Wagner MH (2011) Rheological behavior of lubricating systems in polypropylene/seaweed composites. *J Appl Polym Sci* 121: 2143–2148.
30. Li R, Yu W, Zhou CJ (2006) Rheological characterization of droplet-matrix versus co-continuous morphology. *J Macromol Sci B* 45: 889–898.
31. Ezzati P, Ghasemi I, Karrabi M, et al. (2008) Rheological behaviours of PP/EPDM Blends: The effect of Compatibilization. *Iran Polym J* 17: 669–679.

AIMS Press